Uncertainty Quantification of Turbulence Model Closure Coefficients for Transonic Wall-Bounded Flows

John Schaefer[*]

Missouri University of Science and Technology, Rolla, MO, 65409

Thomas West[†]

NASA Langley Research Center, Hampton, VA 23681

Serhat Hosder[‡]

Missouri University of Science and Technology, Rolla, MO, 65409

Christopher Rumsey,[§] Jan-Renee Carlson,[¶] and William Kleb[‖]

NASA Langley Research Center, Hampton, VA 23681

The goal of this work was to quantify the uncertainty and sensitivity of commonly used turbulence models in Reynolds-Averaged Navier-Stokes codes due to uncertainty in the values of closure coefficients for transonic, wall-bounded flows and to rank the contribution of each coefficient to uncertainty in various output flow quantities of interest. Specifically, uncertainty quantification of turbulence model closure coefficients was performed for transonic flow over an axisymmetric bump at zero degrees angle of attack and the RAE 2822 transonic airfoil at a lift coefficient of 0.744. Three turbulence models were considered: the Spalart-Allmaras Model, Wilcox (2006) k-ω Model, and the Menter Shear-Stress Transport Model. The FUN3D code developed by NASA Langley Research Center was used as the flow solver. The uncertainty quantification analysis employed stochastic expansions based on non-intrusive polynomial chaos as an efficient means of uncertainty propagation. Several integrated and point-quantities are considered as uncertain outputs for both CFD problems. All closure coefficients were treated as epistemic uncertain variables represented with intervals. Sobol indices were used to rank the relative contributions of each closure coefficient to the total uncertainty in the output quantities of interest. This study identified a number of closure coefficients for each turbulence model for which more information will reduce the amount of uncertainty in the output significantly for transonic, wall-bounded flows.

[*]Graduate Student, Department of Aerospace and Mechanical Engineering, Student Member AIAA.
[†]Aerospace Engineer, Vehicle Analysis Branch, Systems Analysis and Concepts Directorate, Member AIAA.
[‡]Associate Professor of Aerospace Engineering, Department of Aerospace and Mechanical Engineering, Senior Member AIAA.
[§]Aerospace Engineer, Computational AeroSciences Branch, Research Directorate, AIAA Fellow.
[¶]Aerospace Engineer, Computational AeroSciences Branch, Research Directorate, Senior Member AIAA.
[‖]Acting Head, Computational AeroSciences Branch, Research Directorate, Lifetime Member AIAA.

American Institute of Aeronautics and Astronautics

Nomenclature

C_D	Drag Coefficient
C_L	Lift Coefficient
C_p	Pressure Coefficient
C_f	Skin Friction Coefficient
M	Mach Number
Re	Reynolds Number
T	Temperature
n	Number of Uncertain Variables
n_p	Oversampling Ratio
N_s	Total Number of Samples
p	Order of Response Surface Polynomial
C_{D_press}	Drag Coefficient due to Pressure
C_{D_sf}	Drag Coefficient due to Skin Friction
α^*	Stochastic Response Function
α_i	Deterministic Component of α^*
Ψ_i	Random Variable Basis Functions of α^*
$\boldsymbol{x}$	Deterministic Vector
$\boldsymbol{\xi}$	Random Variable Vector
D	Total Variance
$S_{i_1...i_s}$	Sobol indices

$\left.\begin{array}{llll} \sigma, & \kappa, & c_{b1}, & c_{b2} \\ c_{v1}, & c_{w2}, & c_{w3}, & c_{t1} \\ c_{t2}, & c_{t3}, & c_{t4} & \end{array}\right\}$ SA Closure Coefficients

$\left.\begin{array}{llll} \sigma_k, & \sigma_w, & \beta^*, & \beta_0 \\ \sigma_{do}, & C_{lim}, & \kappa & \end{array}\right\}$ W2006 Closure Coefficients

$\left.\begin{array}{llll} \sigma_{k1}, & \sigma_{w1}, & \beta_1, & \beta_2 \\ \beta^*, & \sigma_{k2}, & \sigma_{w2}, & \kappa \\ a_1 & & & \end{array}\right\}$ SST Closure Coefficients

u	Velocity
ρ	Density
ν	Molecular Kinematic Viscosity
ν_t	Turbulent Kinematic Viscosity
μ	Molecular Dynamic Viscosity
μ_t	Turbulent Eddy Viscosity
d	Distance from Field Point to Nearest Wall
Ω	Vorticity Magnitude

I. Introduction

Turbulence is one of the greatest unsolved mysteries of classical physics. Due to the highly complex and chaotic nature of the phenomenon, the current physical understanding of turbulence is incomplete. Efforts have been made to create turbulence models to predict turbulent flows by using computational fluid dynamics (CFD); however, the lack of physical knowledge has forced modelers to use dimensional analysis and other methods to identify several constants, called closure coefficients, which balance the model equations. The numerical values of the closure coefficients in current turbulence models are chosen by using a combination of heuristic and empirical decision making. While modelers typically use experimental data to validate their choice of closure coefficients, a turbulence model is not guaranteed to be universally valid for any arbitrary flow.

The goal of this work was to quantify the uncertainty and sensitivity of commonly used turbulence models in Reynolds-Averaged Navier-Stokes (RANS) codes due to uncertainty in the values of closure coefficients for transonic, wall-bounded flows and to rank the contribution of each coefficient to uncertainty in various output flow quantities of interest. Specifically, three turbulence models are considered: the Spalart-Allmaras One-Equation Model (SA),[1] the Wilcox (2006) k-ω Two-Equation Model (W2006),[2] and the Menter Shear-Stress Transport Two-Equation Model (SST).[3] Each model features its own unique set of closure coefficients, which are discussed further in Section III.

Fun3D, an unstructured RANS code of NASA Langley Research Center (LaRC), was chosen as the flow solver for all simulations in this work. More information about Fun3D is included in Section II.A. Two CFD problems are considered in this work. The first is an axisymmetric, transonic bump validation case from Bachalo and Johnson,[4] which is discussed in detail in Section II.B. The second CFD problem is the RAE 2822 transonic airfoil, which is discussed in detail in Section II.C.

To minimize the large computational expense associated with uncertainty quantification of high-fidelity CFD simulations with traditional sampling methods (e.g., Monte Carlo), stochastic expansions based on non-intrusive polynomial chaos (NIPC) are used as an efficient means of uncertainty propagation in this work.[5] All closure coefficients were treated as epistemic uncertain variables (i.e., uncertainty due to lack of knowledge and not due to inherent, systemic uncertainty). Sobol indices,[6] which are global nonlinear

sensitivity indices based on variance decomposition, were used to rank the relative contributions of each closure coefficient to the total uncertainty in the output quantities of interest. For the transonic bump, the output quantities of interest are drag coefficient, pressure coefficient, skin friction coefficient, and separation bubble size. For the RAE 2822, the output quantities of interest are lift coefficient, pressure and skin friction components of drag coefficient, and pressure coefficient.

In Section II, an overview of the flow solver and CFD test problems is presented. In Section III, the details of each of the turbulence models considered here are discussed. A summary of the closure coefficients and their domains is presented for each model. In Section IV, the Uncertainty Quantification (UQ) analysis and computational expense is discussed in further detail. In Section V, the results of all UQ analyses are presented. Finally in Section VI, conclusions are made and some suggestions for future work are presented.

II.   Flow Solver and CFD Test Problems

In this section, the flow solver and CFD test problems are discussed. First, the details of the selected solver are provided. Next information is given for the freestream conditions and meshes of each CFD test problem.

II.A.   Flow Solver

All flow solutions in this work were obtained by using a modified form of FUN3D version 12.4.[7] FUN3D is an unstructured, node-based, three-dimensional, finite-volume RANS code capable of solving steady and unsteady laminar or turbulent flows with subsonic to hypersonic speeds. The modifications to the code were performed to allow changes to the values of turbulence model closure coefficients in the uncertainty analyses. All solutions used a Roe, second-order flux differencing scheme with no flux limiter and second-order spatial accuracy for the viscous terms. The CFL numbers for the mean flow and turbulence model equations were ramped from 10 to 50 and from 5 to 30, respectively, across 500 iterations, and then the CFL numbers were fixed at their maximum values until steady-state convergence was achieved.

II.B.   Problem 1: Axisymmetric Transonic Bump

The first CFD problem considered in this work is an axisymmetric transonic bump validation case from Bachalo and Johnson.[4] The test article in the experiment consisted of a thin-walled cylinder that extended 61 cm upstream of the bump's leading edge, and the cylinder had an outside diameter of 15.2 cm with a bump chord of 20.32 cm. The flow has freestream $M = 0.875$, $T = 540$ °R, and $Re = 2.763 \times 10^6$ (based on the bump length of $c = 1$). All flow solutions were obtained by using the 721 x 321 grid from the NASA Langley Research Center turbulence modeling resource website.[8] The mesh contains 462,882 nodes, 1,155,121 edges, and 230,400 hexahedral cells. It consists of a 1° wedge rotated about the x-axis. The sides of the mesh are treated as periodic interfaces; they are periodic with each other and rotated through 1° in order to simulate axisymmetry. The surface of the bump and cylinder has a solid wall boundary condition, and all other boundary conditions are farfield Riemann. A graphical overview of the axisymmetric transonic bump problem is included in Fig. 1. The circles below the mesh in the figure represent the axisymmetry about the x-axis. An example pressure contour plot is included in Fig. 2 for the transonic bump case obtained with the SA baseline model.

II.C.   Problem 2: RAE 2822 Transonic Airfoil

The second CFD problem considered in this work is the RAE 2822 transonic airfoil at a lift coefficient of 0.744. The experimental data for this case is from Cook and McDonald.[9] The flow has freestream $M = 0.729$, $T = 540$ °R, and $Re = 6.5 \times 10^6$ (based on the airfoil chord of $c = 1$). Numerical integration of the experimental pressure coefficient data yields a lift coefficient of $C_L = 0.744$; the angle of attack was adjusted for each baseline turbulence model to match this value, and all subsequent simulations for each model used the same angle of attack as the one found for the baseline. All flow solutions were obtained by using a 513 x 161 grid containing 206,272 nodes, 514,208 edges, and 102,400 hexahedral cells. The grid is a 2D C-mesh extruded one unit in the y-direction with y-symmetry boundary conditions on either side and with a solid wall boundary condition on the airfoil surface. All other boundary conditions are farfield
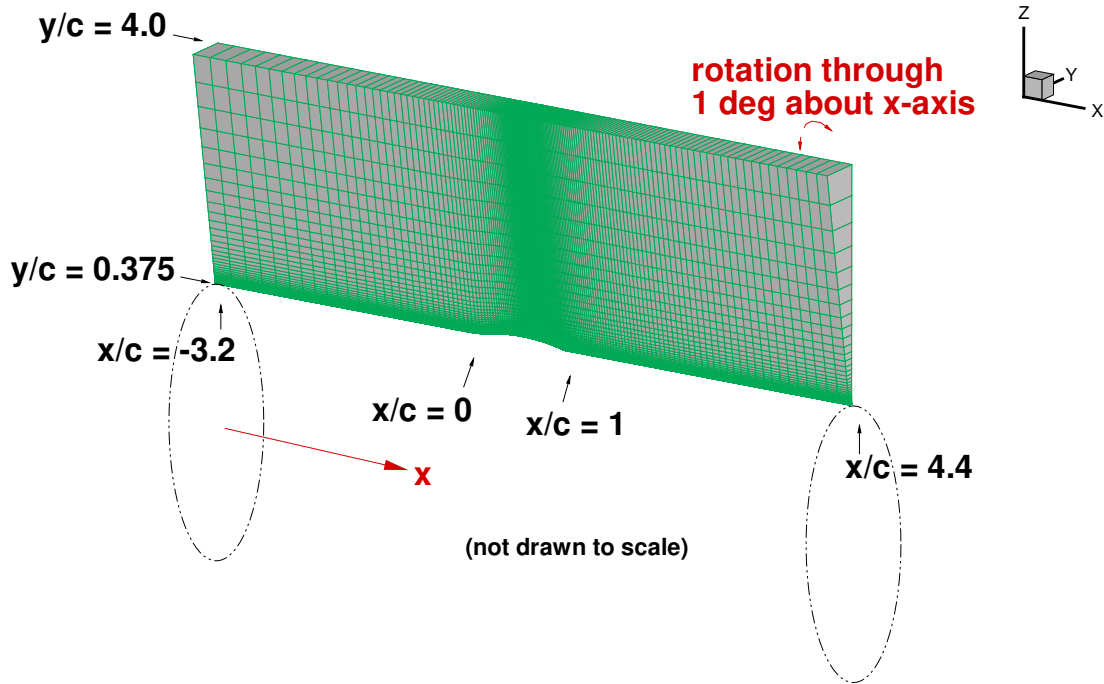
Figure 1. Axisymmetric transonic bump overview from Ref. 8.

Riemann. A graphical view of the RAE 2822 grid is included in Fig. 3. An example pressure contour plot is included in Fig. 4, which was obtained with the SA baseline model.

III.   Turbulence Models

In this section, the details of the turbulence models employed in this work are outlined. Each subsection contains an overview of a turbulence model, its closure coefficient values, and estimates of the epistemic intervals for each closure coefficient. Note that the two-equation turbulence model equations are written in conserved variable form, but the flow solutions are calculated with primitive variable form. Note that in this work, the nomenclature from the NASA LaRC turbulence modeling website[8] is used.
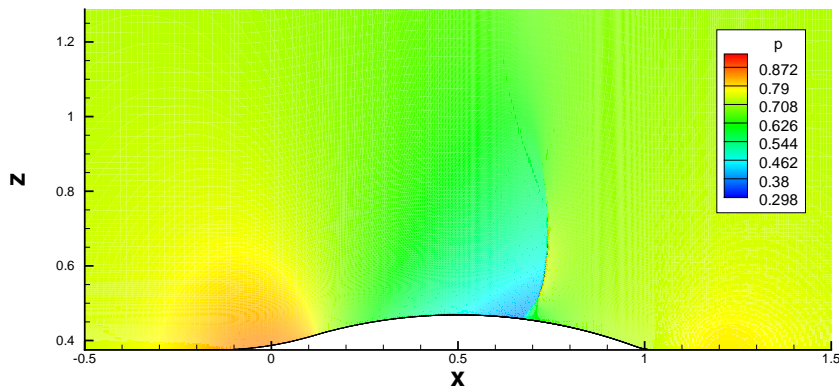

Figure 2. Non-dimensional pressure contours (scaled with the freestream value) of axisymmetric transonic bump.

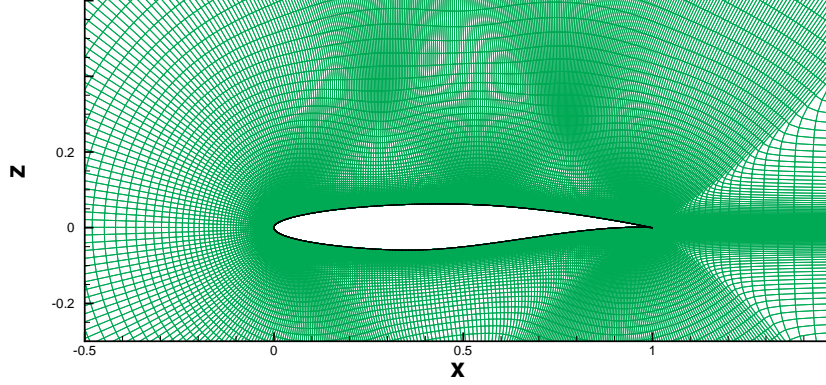American Institute of Aeronautics and Astronautics

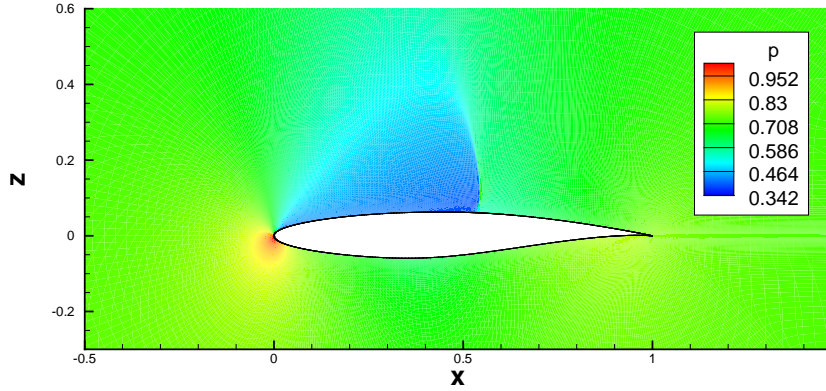Figure 3. The computational grid around the RAE 2822 transonic airfoil.

Figure 4. Non-dimensional pressure contours (scaled with the freestream value) of RAE 2822 Airfoil.

III.A. Spalart-Allmaras One-Equation Model (SA)

The SA model was developed as an evolution of the Nee-Kovasznay model,[10] but with several near-wall and compressibility corrections.[1] It is simpler, less computationally expensive, and more computationally robust than multi-equation models, and it is widely used for aerodynamic flows in engineering applications. The model is given by

$$\frac{\partial \hat{\nu}}{\partial t} + u_j \frac{\partial \hat{\nu}}{\partial x_j} = c_{b1}\left(1 - f_{t2}\right)\hat{S}\hat{\nu} - \left[c_{w1}f_w - \frac{c_{b1}}{\kappa^2}f_{t2}\right]\left(\frac{\hat{\nu}}{d}\right)^2 + \frac{1}{\sigma}\left[\frac{\partial}{\partial x_j}\left((\nu + \hat{\nu})\frac{\partial \hat{\nu}}{\partial x_j}\right) + c_{b2}\frac{\partial \hat{\nu}}{\partial x_i}\frac{\partial \hat{\nu}}{\partial x_i}\right] \quad (1)$$

The full formulation of the model is given by Spalart and Allmaras.[1] The closure coefficients and their suggested values are given in Table 1. The closure coefficients also include

$$c_{w1} = \frac{c_{b1}}{\kappa^2} + \frac{1 + c_{b2}}{\sigma} \quad (2)$$

The turbulent eddy viscosity is computed from:

$$\mu_t = \rho \hat{\nu} f_{v1} \quad (3)$$

where

$$f_{v1} = \frac{\chi^3}{\chi^3 + c_{v1}^3}, \quad \chi = \frac{\hat{\nu}}{\nu} \quad (4)$$

American Institute of Aeronautics and Astronautics

and ρ is the density, $\nu = \mu/\rho$ is the molecular kinematic viscosity, and μ is the molecular dynamic viscosity. Additional definitions are given by the following equations:

$$\hat{S} = \Omega + \frac{\hat{\nu}}{\kappa^2 d^2} f_{\nu 2} \tag{5}$$

where $\Omega = \sqrt{2W_{ij}W_{ij}}$ is the magnitude of the vorticity, d is the distance from the field point to the nearest wall, and

$$
\begin{aligned}
f_{v2} &= 1 - \frac{\chi}{1 + \chi f_{\nu 1}}, & f_w &= g \left[\frac{1 + c_{w3}^6}{g^6 + c_{w3}^6} \right]^{1/6}, & g &= r + c_{w2} \left(r^6 - r \right) \\
r &= \min \left[\frac{\hat{\nu}}{\hat{S}\kappa^2 d^2}, 10 \right], & f_{t2} &= c_{t3} \exp \left(-c_{t4}\chi^2 \right), & W_{ij} &= \frac{1}{2} \left(\frac{\partial u_i}{\partial x_j} - \frac{\partial u_j}{\partial x_i} \right)
\end{aligned} \tag{6}
$$

According to Spalart and Allmaras,[1] the following constraints should be enforced:

$$\sigma \in [0.6, 1.0] \tag{7}$$
$$c_{t1} \in [0.1, 10] \tag{8}$$
$$c_{t3} > 1.0 \tag{9}$$
$$c_{v1} > 6.9 \tag{10}$$

Spalart and Allmaras also note in Ref. 1 that c_{t2} is "not a candidate for much adjustment," and that c_{t4} can be decreased some, but that "values much smaller than 1 would start affecting the results in the turbulent region." Bailey et al.[11] determined that $\kappa = 0.40 \pm 0.02$ in their turbulent pipe flow experiments, and this range of κ was used for all of the turbulence models examined in this work. In private communication with the first author,[12] Spalart recommended using the bounds of Fig. 1 in Ref. 1 to determine the epistemic intervals of c_{b1}, c_{b2}, and c_{w2}. Spalart also recommended that

$$c_{w3} \in [1.75, 2.5] \tag{11}$$

In total, eleven closure coefficients were varied in the UQ analysis for SA. A summary of the SA closure coefficients to be varied, and their associated epistemic intervals are included in Table 1.

III.B. Wilcox (2006) k-ω Two-Equation Model (W2006)

The k-ω model utilizes two equations to model a turbulent kinetic energy and length scale determining variable. The first equation is for turbulent kinetic energy, k, and the second equation is for the dissipation per unit turbulence kinetic energy, ω. In 2006, Wilcox introduced a new version of the k-ω model which

Table 1. SA Closure Coefficients and Associated Epistemic Intervals.

Coefficient	Standard Value	Lower Bound	Upper Bound
σ	2/3	0.6	1.0
κ	0.41	0.38	0.42
c_{v1}	7.1	6.9	7.3
c_{w3}	2.0	1.75	2.5
c_{t1}	1.0	0.1	10.0
c_{t2}	2.0	1.9	2.1
c_{t3}	1.2	1.0	2.0
c_{t4}	0.5	0.3	0.7
c_{b1}	0.1355	0.12893	0.13700
c_{b2}	0.622	0.60983	0.68750
c_{w2}	0.3	0.05500	0.35250

American Institute of Aeronautics and Astronautics

greatly improved its accuracy for free shear flows and strongly separated flows by introducing a cross-diffusion term and a built-in stress-limiter.[13] The W2006 model is given by

$$\frac{\partial(\rho k)}{\partial t} + \frac{\partial(\rho u_j k)}{\partial x_j} = P - \beta^* \rho \omega k + \frac{\partial}{\partial x_j}\left[\left(\mu + \sigma_k \frac{\rho k}{\omega}\right)\frac{\partial k}{\partial x_j}\right] \tag{12}$$

$$\frac{\partial(\rho \omega)}{\partial t} + \frac{\partial(\rho u_j \omega)}{\partial x_j} = \frac{\gamma \omega}{k} P - \beta \rho \omega^2 + \frac{\partial}{\partial x_j}\left[\left(\mu + \sigma_w \frac{\rho k}{\omega}\right)\frac{\partial \omega}{\partial x_j}\right] + \frac{\rho \sigma_d}{\omega}\frac{\partial k}{\partial x_j}\frac{\partial \omega}{\partial x_j} \tag{13}$$

The full formulation of the model is given by Wilcox.[2] The closure coefficients and their suggested values are given in Table 2. The closure coefficients also include

$$\gamma = \frac{\beta_0}{\beta^*} - \sigma_w \frac{\kappa^2}{\sqrt{\beta^*}} \tag{14}$$

Definitions of the terms in the model include:

$$P = \tau_{ij}\frac{\partial u_i}{\partial x_j} \tag{15}$$

$$\tau_{ij} = \mu_t\left(2S_{ij} - \frac{2}{3}\frac{\partial u_k}{\partial x_k}\delta_{ij}\right) - \frac{2}{3}\rho k \delta_{ij} \tag{16}$$

$$S_{ij} = \frac{1}{2}\left(\frac{\partial u_i}{\partial x_j} + \frac{\partial u_j}{\partial x_i}\right) \tag{17}$$

and the turbulent eddy viscosity is computed from:

$$\mu_t = \frac{\rho k}{\hat{\omega}} \tag{18}$$

where:

$$\hat{\omega} = \max\left[\omega,\ C_{lim}\sqrt{\frac{2\bar{S}_{ij}\bar{S}_{ij}}{\beta^*}}\right] \tag{19}$$

$$\bar{S}_{ij} = S_{ij} - \frac{1}{3}\frac{\partial u_k}{\partial x_k}\delta_{ij} \tag{20}$$

The auxiliary functions are

$$\chi_\omega = \left|\frac{\Omega_{ij}\Omega_{jk}\hat{S}_{ki}}{(\beta^*\omega)^3}\right|, \qquad f_\beta = \frac{1 + 85\chi_\omega}{1 + 100\chi_\omega}, \quad \sigma_d = \begin{cases} 0, & \frac{\partial k}{\partial x_j}\frac{\partial \omega}{\partial x_j} \le 0 \\[2mm] \sigma_{do}, & \frac{\partial k}{\partial x_j}\frac{\partial \omega}{\partial x_j} > 0 \end{cases} \tag{21}$$

$$\hat{S}_{ki} = S_{ki} - \frac{1}{2}\frac{\partial u_m}{\partial x_m}\delta_{ki}, \quad \Omega_{ij} = \frac{1}{2}\left(\frac{\partial u_i}{\partial x_j} - \frac{\partial u_j}{\partial x_i}\right)$$

In Ref. 13, Wilcox states that $\tau_{xy}/k \approx 3/10$, so $\beta^* = (\tau_{xy}/k)^2 \approx 9/100$. From this description, the author assumed that $\tau_{xy}/k \in [0.28, 0.32]$, yielding $\beta^* \in [0.0784, 0.1024]$. Wilcox also states that $\beta^*/\beta_0 = 1.25 \pm 0.06$ and that the following inequalities must hold true:

$$\sigma_{do} > \sigma_k - \sigma_w \tag{22}$$

$$\sigma_k > \sigma_{do} \tag{23}$$

In this study, the standard value of 1/8 was used for σ_{do} in all flow solutions. Acceptable ranges for σ_w and σ_k were established from inequalities (22) and (23) and from Figs. 4.16 and 4.17 in Ref. 13. In private communication with the first author,[14] Wilcox stated that the standard value of C_{lim} was chosen mainly for applications with Mach number greater than two. For the transonic range, Wilcox recommended a value of C_{lim} closer to one.

In total, six closure coefficients were varied in the UQ analysis for W2006. A summary of the W2006 closure coefficients to be varied and their epistemic intervals are included in Table 2.

Table 2. W2006 Closure Coefficients and Associated Epistemic Intervals.

Coefficient	Standard Value	Lower Bound	Upper Bound
β^*	0.09	0.0784	0.1024
C_{lim}	0.875	0.75	1.0
κ	0.40	0.38	0.42
β^*/β_0	1.2712	1.19	1.31
σ_w	0.5	0.5	0.7
σ_k	0.6	0.5	0.6

III.C.   Menter Shear-Stress Transport Two-Equation Model (SST)

Menter's SST model uses blending functions to combine the k-ω and k-ϵ models.[3] The objective is to use the k-ω model in the near wall region where it is most accurate, and to take advantage of the freestream independence of the k-ϵ model in the outer part of the boundary layer. The model is given by

$$\frac{\partial(\rho k)}{\partial t} + \frac{\partial(\rho u_j k)}{\partial x_j} = P - \beta^* \rho \omega k + \frac{\partial}{\partial x_j}\left[(\mu + \sigma_k \mu_t)\frac{\partial k}{\partial x_j}\right] \tag{24}$$

$$\frac{\partial(\rho \omega)}{\partial t} + \frac{\partial(\rho u_j \omega)}{\partial x_j} = \frac{\gamma}{\nu_t} P - \beta \rho \omega^2 + \frac{\partial}{\partial x_j}\left[(\mu + \sigma_w \mu_t)\frac{\partial \omega}{\partial x_j}\right] + 2(1-F_1)\frac{\rho \sigma_{w2}}{\omega}\frac{\partial k}{\partial x_j}\frac{\partial \omega}{\partial x_j} \tag{25}$$

The full formulation of the model is given by Menter.[3] The closure coefficients and their suggested values are given in Table 3. The closure coefficients also include

$$\gamma_1 = \frac{\beta_1}{\beta^*} - \sigma_{w1}\frac{\kappa^2}{\sqrt{\beta^*}} \tag{26}$$

$$\gamma_2 = \frac{\beta_2}{\beta^*} - \sigma_{w2}\frac{\kappa^2}{\sqrt{\beta^*}} \tag{27}$$

As in the W2006 model, P, τ_{ij}, and S_{ij} are given by:

$$P = \tau_{ij}\frac{\partial u_i}{\partial x_j} \tag{28}$$

$$\tau_{ij} = \mu_t\left(2S_{ij} - \frac{2}{3}\frac{\partial u_k}{\partial x_k}\delta_{ij}\right) - \frac{2}{3}\rho k \delta_{ij} \tag{29}$$

$$S_{ij} = \frac{1}{2}\left(\frac{\partial u_i}{\partial x_j} + \frac{\partial u_j}{\partial x_i}\right) \tag{30}$$

but the turbulent eddy viscosity is computed from:

$$\mu_t = \frac{\rho a_1 k}{\max(a_1 \omega,\ \Omega F_2)} \tag{31}$$

Each of the constants is a blend of an inner (1) and outer (2) constant, blended via

$$\phi = F_1 \phi_1 + (1-F_1)\phi_2 \tag{32}$$

where ϕ_1 represents constant 1 and ϕ_2 represents constant 2. Additional functions are given by

$$
\begin{aligned}
F_1 &= \tanh(arg_1^4), & arg_1 &= \min\left[\max\left(\frac{\sqrt{k}}{\beta^* \omega d}, \frac{500\nu}{d^2 \omega}\right), \frac{4\rho \sigma_{\omega 2} k}{CD_{k\omega} d^2}\right] \\[2mm]
\nu_t &= \frac{\mu_t}{\rho}, & CD_{k\omega} &= \max\left(2\rho \sigma_{\omega 2}\frac{1}{\omega}\frac{\partial k}{\partial x_j}\frac{\partial \omega}{\partial x_j},\ 10^{-20}\right) \\[2mm]
F_2 &= \tanh(arg_2^2), & arg_2 &= \max\left(2\frac{\sqrt{k}}{\beta^* \omega d}, \frac{500\nu}{d^2 \omega}\right) \\[2mm]
\Omega &= \sqrt{2W_{ij}W_{ij}}, & W_{ij} &= \frac{1}{2}\left(\frac{\partial u_i}{\partial x_j} - \frac{\partial u_j}{\partial x_i}\right)
\end{aligned}
\tag{33}
$$

American Institute of Aeronautics and Astronautics

Table 3. SST Closure Coefficients and Associated Epistemic Intervals.

Coefficient	Standard Value	Lower Bound	Upper Bound
σ_{k1}	0.85	0.7	1.0
σ_{k2}	1.0	0.8	1.2
σ_{w1}	0.5	0.3	0.7
σ_{w2}	0.856	0.7	1.0
β^*/β_1	1.20	1.19	1.31
β^*/β_2	1.0870	1.05	1.45
β^*	0.09	0.0784	0.1024
κ	0.41	0.38	0.42
a_1	0.31	0.31	0.40

where ρ is the density, ν_t is the turbulent kinematic viscosity, μ is the dynamic viscosity, d is the distance from the field point to the nearest wall, and Ω is the vorticity magnitude.

Menter states that, "It has been the author's experience that small changes (5-10%) in modeling constraints can lead to a significant improvement (or deterioration) of model predictions."[3] Unfortunately, little more information is available regarding plausible domains for SST closure coefficients. Many of the SST closure coefficients are shared with W2006, and in these cases the same epistemic intervals from W2006 were employed for SST. Georgiadis and Yoder[15] determined that $a_1 \in [0.31, 0.40]$. Menter agreed with this assessment in private communication with the first author,[16] stating that "One can only increase a_1 — decreasing it interferes with the log layer calibration."

In total, nine closure coefficients were varied in the UQ analysis for SST. A summary of the SST closure coefficients to be varied and their epistemic intervals is included in Table 3.

IV. Uncertainty Quantification Approach

Uncertainties in computational models fall into two categories: aleatory and epistemic. Aleatory uncertainties represent inherent variations in a system, whereas epistemic uncertainties arise due to lack of knowledge. (For example, the outcome of a coin flip is aleatory because it is due to inherent chance; however if a coin is placed on a table and covered up, the uncertainty in heads/tails is epistemic because it is due to a lack of knowledge.) In this work, all closure coefficients are treated as epistemic uncertain variables due to the lack of a complete physical understanding of turbulence.

Rather than resorting to Monte Carlo simulations for uncertainty quantification, stochastic expansions based on Point-Collocation Non-Intrusive Polynomial Chaos (NIPC) were employed to reduce computational expense.[5] The strategy of Point-Collocation NIPC is to create a surrogate model via least squares approach (i.e., polynomial response surface) by using the CFD output obtained at a number of Latin Hypercube sample points for the propagation of uncertainty. An explanation of Point-Collocation NIPC given by West et al.[17] follows. With the polynomial chaos approach, a stochastic response function α^* (e.g., drag coefficient, pressure or skin friction coefficient at a given point in the flow field) can be decomposed into separable deterministic and stochastic components within a series expansion:

$$\alpha^*(\boldsymbol{x}, \boldsymbol{\xi}) \approx \sum_{i=0}^{P} \alpha_i(\boldsymbol{x})\Psi_i(\boldsymbol{\xi}) \tag{34}$$

where α_i is the deterministic component and Ψ_i is the random variable basis functions corresponding to the ith mode. α^* is assumed to be a function of a deterministic vector $\boldsymbol{x}$, which includes the spatial coordinates and deterministic parameters of the problem, and of the n-dimensional standard random variable vector $\boldsymbol{\xi}$. In theory, the series in Eq. (34) is infinite, but for practical implementation of the polynomial chaos expansions it is truncated and a discrete sum is taken over a number of output modes, $(P + 1)$. Further details on polynomial chaos theory are given by Ghanem[18] and Eldred.[19]

There are three parameters that determine the number of samples required to generate the response surface: the number of uncertain variables, n; the order of the response surface polynomial, p; and the

oversampling ratio, n_p. The total number of samples, N_s, is then given by

$$N_s = n_p \cdot (P + 1) = n_p \left[\frac{(n + p)!}{n!p!} \right] \tag{35}$$

The Point-Collocation NIPC method starts with replacing a stochastic response or random function with its polynomial chaos expansion in Eq. (34). Then, N_s vectors are chosen in random space and the deterministic code (the CFD flow solver in this case) is evaluated at these points; this is the left-hand side of Eq. (34). Finally a linear system of N_s equations is formulated and solved for the spectral modes of the random variables. This system is given by:

$$\begin{pmatrix} \alpha^*(\boldsymbol{x}, \boldsymbol{\xi}_0) \\ \alpha^*(\boldsymbol{x}, \boldsymbol{\xi}_1) \\ \vdots \\ \alpha^*(\boldsymbol{x}, \boldsymbol{\xi}_{(N_s-1)}) \end{pmatrix} = \begin{pmatrix} \Psi_0(\boldsymbol{\xi}_0) & \Psi_1(\boldsymbol{\xi}_0) & \dots & \Psi_P(\boldsymbol{\xi}_0) \\ \Psi_0(\boldsymbol{\xi}_1) & \Psi_1(\boldsymbol{\xi}_1) & \dots & \Psi_P(\boldsymbol{\xi}_1) \\ \vdots & \vdots & \ddots & \vdots \\ \Psi_0(\boldsymbol{\xi}_{(N_s-1)}) & \Psi_1(\boldsymbol{\xi}_{(N_s-1)}) & \dots & \Psi_P(\boldsymbol{\xi}_{(N_s-1)}) \end{pmatrix} \begin{pmatrix} \alpha_0 \\ \alpha_1 \\ \vdots \\ \alpha_P \end{pmatrix} \tag{36}$$

An oversampling ratio of 1.0 yields the minimum number of samples required to produce a response surface. Hosder et al.[20] demonstrated that an oversampling ratio of $n_p = 2.0$ gives a better approximation to the statistics at each polynomial degree they considered. For this reason, $n_p = 2.0$ was used for all of the UQ analyses in this work. Given $n_p > 1.0$, Eq. (36) is overdetermined and can be solved using a least squares approach. In the current work, a polynomial order of two ($p = 2$) was used for all UQ analyses.

Sobol indices (global nonlinear sensitivity indices) were used to rank the relative contributions of each closure coefficient to the total uncertainty in the output quantities of interest. Sobol indices can be derived via Sobol Decomposition, which is a variance-based global sensitivity analysis method. This derivation utilizes the polynomial chaos expansion coefficients calculated in Eq. (36), and is included in Appendix A.

Due to the bounded nature of epistemic input uncertainties, Legendre polynomials are used in this study as the basis functions. Although stochastic response surfaces created with the NIPC approach allow the calculation of confidence intervals along with various statistics of the output for probabilistic (aleatory) input, in this study only the maximum and the minimum of the response will be calculated from the response surface to determine the epistemic interval for each uncertain output.

Initially all of the closure coefficients in Tables 1, 2, and 3 were used in the uncertainty quantification analyses. The results of these analysis are presented in the next section. The closure coefficients that contribute most to the uncertain outputs in the original analyses are then used as the uncertain variables in a second set of reduced-dimensionality analyses (RDA). The objective of the second set of analyses is to obtain more accurate response surfaces and Sobol indices for the significant closure coefficients. A summary of the computational cost (i.e., number of CFD evaluations required) of the transonic bump analyses is included in Table 4, and a summary of the computational cost of the RAE 2822 analyses is included in Table 5.

V.   Results

The results of all uncertainty quantification analyses are presented in this section. The axisymmetric, transonic bump is discussed in Sections V.A and V.B; and the RAE 2822 transonic airfoil is discussed in Sections V.C and V.D. Finally, a comparison of the results from both CFD problems is discussed in Section V.E.

Table 4.   Number of CFD Evaluations Required for Transonic Bump UQ Analyses.

Turbulence Model	Original Analysis				RDA			
	n	p	n_p	N_s	n	p	n_p	N_s
SA	11	2	2	156	6	2	2	56
W2006	6	2	2	56	3	2	2	20
SST	9	2	2	110	5	2	2	42

Table 5. Number of CFD Evaluations Required for RAE 2822 UQ Analyses.

Turbulence Model	Original Analysis				RDA			
	n	p	n_p	N_s	n	p	n_p	N_s
SA	11	2	2	156	7	2	2	72
W2006	6	2	2	56	3	2	2	20
SST	9	2	2	110	5	2	2	42

V.A. Axisymmetric Transonic Bump - Original Analyses

The purpose of the original uncertainty quantification analyses was to identify the closure coefficients that contribute significantly to uncertainty in the output quantities of interest. These coefficients were later used in reduced-dimensionality analyses. For the transonic bump, the output quantities of interest include drag coefficient (C_D); pressure and skin friction coefficient distributions (C_p and C_f); and separation bubble size.

Sobol indices were used to rank the relative contributions of each closure coefficient to the overall uncertainty in C_D. Coefficients with higher Sobol indices contribute more to the uncertainty than coefficients with lower Sobol indices. The Sobol indices of the closure coefficients for each turbulence model for C_D are presented in Table 6, where they are ranked from highest to lowest. The largest contributors to uncertainty in each model are typed in blue. Coefficients with Sobol indices of less than $3.0{\times}10^{-2}$ were not considered to be significant. The closure coefficients retained for each turbulence model with this approach account for at least 95% of the total uncertainty in the output quantity of interest (Table 6).

**Table 6. Sobol Indices of Closure Coefficients for C_D.**

SA		W2006		SST	
Coefficient	Sobol Index	Coefficient	Sobol Index	Coefficient	Sobol Index
κ	$8.50{\times}10^{-1}$	σ_w	$7.75{\times}10^{-1}$	β^*	$8.03{\times}10^{-1}$
σ	$5.99{\times}10^{-2}$	C_{lim}	$1.42{\times}10^{-1}$	σ_{w1}	$9.24{\times}10^{-2}$
c_{v1}	$5.38{\times}10^{-2}$	β^*	$1.26{\times}10^{-1}$	β^*/β_1	$7.79{\times}10^{-2}$
c_{w2}	$2.59{\times}10^{-2}$	σ_k	$2.12{\times}10^{-2}$	β^*/β_2	$3.54{\times}10^{-2}$
c_{b1}	$1.11{\times}10^{-2}$	κ	$1.99{\times}10^{-2}$	σ_{w2}	$1.85{\times}10^{-3}$
c_{b2}	$4.66{\times}10^{-4}$	β^*/β_0	$7.46{\times}10^{-3}$	σ_{k2}	$1.21{\times}10^{-3}$
c_{w3}	$5.33{\times}10^{-5}$			a_1	$8.25{\times}10^{-4}$
c_{t3}	$9.71{\times}10^{-6}$			σ_{k1}	$4.91{\times}10^{-4}$
c_{t1}	$8.91{\times}10^{-6}$			κ	$1.24{\times}10^{-4}$
c_{t4}	$8.57{\times}10^{-6}$				
c_{t2}	$5.13{\times}10^{-6}$				

The largest contributors to uncertainty in C_D for the SA model are κ, σ, and c_{v1}. The largest contributors for W2006 are σ_w, C_{lim}, and β^*. The largest contributors for SST are β^*, σ_{w1}, β^*/β_1, and β^*/β_2. Note that β^* is shared by both the W2006 and SST models. Also note that σ_{w1} in the SST model is the equivalent of σ_w in the W2006 model. Von Kármán's constant (κ) is included in all three models, but it is only significant to uncertainty in C_D for the SA model.

Response surfaces for pressure coefficient (C_p) and skin friction coefficient (C_f) were generated at each axial location across the bump. Sobol indices for these coefficients were also calculated at each axial location. Plots of the Sobol indices for C_p and C_f versus x were generated so that the closure coefficients significant to these quantities at points in the flow could be identified. These plots are included in Fig. 5. For clarity, only the Sobol indices of coefficients with significant contributions to uncertainty in C_p are shown in the plots.

The largest contributors to uncertainty in C_p and C_f for the SA model are σ, κ, c_{v1}, c_{w3}, c_{b1}, and c_{w2}. The largest contributors for the W2006 model are β^*, C_{lim}, and σ_w. The largest contributors for the SST model are σ_{w1}, β^*/β_1, β^*/β_2, β^*, and a_1.
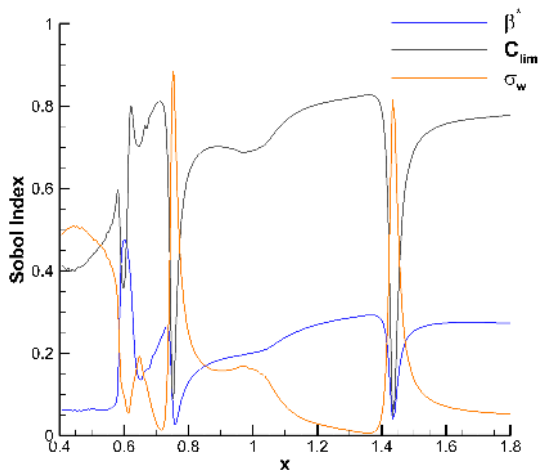
The separation bubble size for each case of each model was taken as the difference between the x-coordinate of the zero-intersection points in the C_f versus x curves. Using the same process as before,
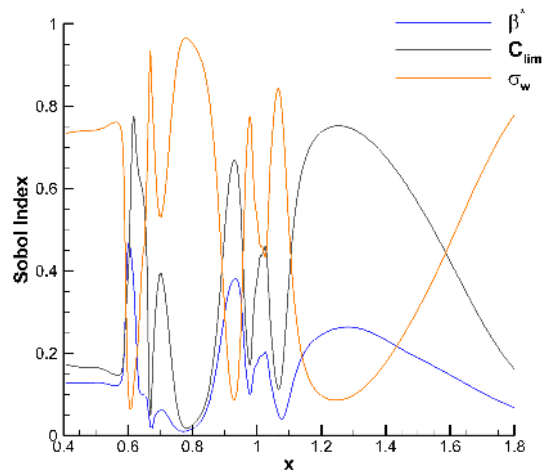
American Institute of Aeronautics and Astronautics
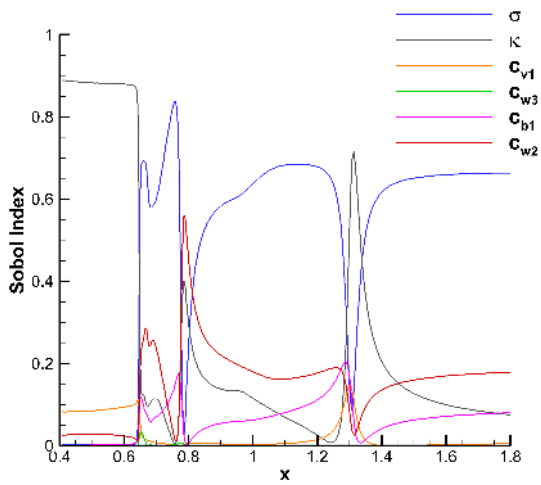
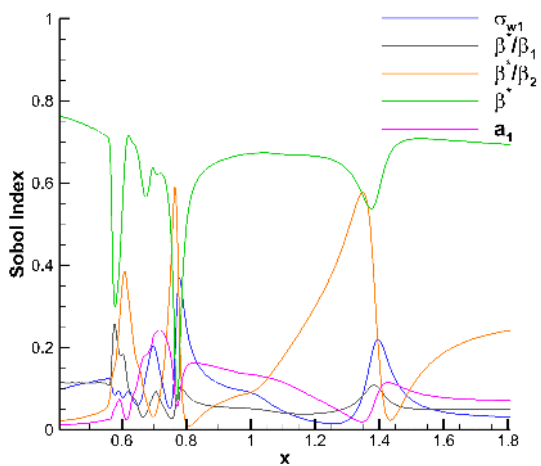(a) Sobol indices for C_p versus x (SA).
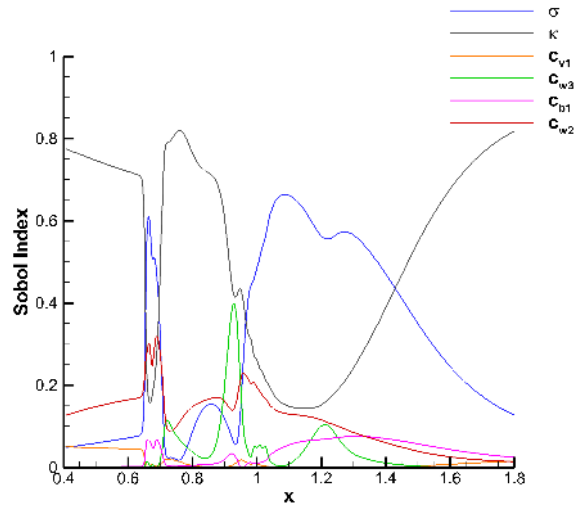
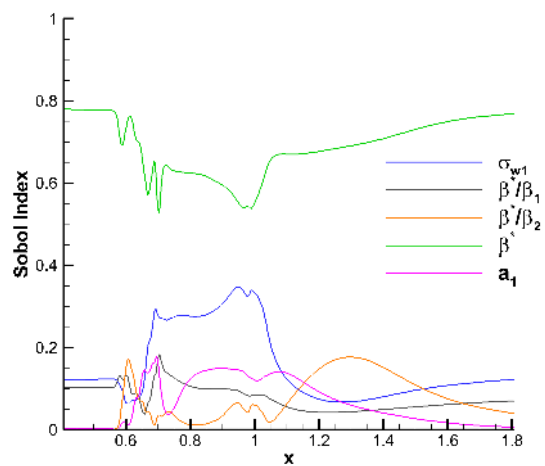(b) Sobol indices for C_f versus x (SA).

(c) Sobol indices for C_p versus x (W2006).

(d) Sobol indices for C_f versus x (W2006).

(e) Sobol indices for C_p versus x (SST).

(f) Sobol indices for C_f versus x (SST).

Figure 5. Sobol index distributions for transonic bump (Original Analyses).

Table 7. Sobol Indices of Closure Coefficients for Separation Bubble Size.

SA		W2006		SST	
Coefficient	Sobol Index	Coefficient	Sobol Index	Coefficient	Sobol Index
σ	5.58×10^{-1}	C_{lim}	7.26×10^{-1}	β^*	6.49×10^{-1}
κ	1.82×10^{-1}	β^*	2.57×10^{-1}	σ_{w1}	1.15×10^{-1}
c_{w2}	1.54×10^{-1}	σ_w	1.03×10^{-1}	a_1	1.06×10^{-1}
c_{b1}	6.74×10^{-2}	σ_k	1.46×10^{-2}	β^*/β_2	9.48×10^{-2}
c_{w3}	3.71×10^{-2}	κ	9.92×10^{-3}	β^*/β_1	9.24×10^{-2}
c_{v1}	1.87×10^{-3}	β^*/β_0	5.51×10^{-3}	σ_{k2}	2.09×10^{-2}
c_{t3}	6.76×10^{-4}			κ	1.70×10^{-2}
c_{t4}	6.05×10^{-4}			σ_{w2}	1.36×10^{-2}
c_{t2}	5.98×10^{-4}			σ_{k1}	9.77×10^{-3}
c_{b2}	5.68×10^{-4}				
c_{t1}	5.56×10^{-4}				

Table 8. Closure Coefficients with Significant Contributions to Transonic Bump.

SA	W2006	SST
σ	β^*	σ_{w1}
κ	C_{lim}	β^*/β_1
c_{v1}	σ_w	β^*/β_2
c_{w2}		β^*
c_{b1}		a_1
c_{w3}		

stochastic response surfaces were created for the separation bubble size for each model. The Sobol indices of the closure coefficients for separation bubble size are given in Table 7.

The largest contributors to uncertainty in separation bubble size for the SA model are σ, κ, c_{w2}, c_{b1}, and c_{w3}. The largest contributors for the W2006 model are C_{lim}, β^*, and σ_w. The largest contributors for the SST model are β^*, σ_{w1}, a_1, β^*/β_2, and β^*/β_1.

In sum, six closure coefficients were found to contribute significantly to at least one output quantity of interest for the SA model; three closure coefficients for the W2006 model; and five coefficients for the SST model. This information is summarized in Table 8.

V.B.   Axisymmetric Transonic Bump - Reduced Dimensionality Analyses

To further increase the accuracy of the uncertainty analysis by creating the stochastic response surface with a smaller number of uncertain variables, a reduced dimensionality analysis (RDA) was performed for the axisymmetric transonic bump with each turbulence model by using only the significant closure coefficients found in Table 8.

A baseline case was run with the standard set of closure coefficients for each turbulence model. Stochastic polynomial response surfaces of C_D were obtained with NIPC on the uncertain domain. The minimum and maximum values of drag coefficient (C_D) for each model were calculated from these response surfaces. To verify the accuracy of each response surface, additional CFD solutions were generated by using the sets of closure coefficients that produced the minimum and maximum values of C_D on the response surface; the C_D comparison between the response surfaces and the CFD is summarized in Table 9. In each case, the response surface is within 4.07% or less of the CFD. The difference values reported in Table 9 indicate an acceptable level of accuracy for epistemic uncertainty analyses.

In the experiment, Bachalo and Johnson estimated the separation and reattachment points to be $x = 0.70$ and $x = 1.1$ respectively. This yields a separation bubble size of $0.40(x/c)$ (based on the bump length of

Table 9. Drag Coefficient Results, in Drag Counts (RDA).

Model	Baseline C_D CFD	Min C_D Resp. Surf.	CFD	Difference	Max C_D Resp. Surf.	CFD	Difference
SA	2.232	2.148	2.130	0.85%	2.270	2.288	0.79%
W2006	2.226	2.116	2.098	0.86%	2.243	2.224	0.85%
SST	2.284	1.813	1.890	4.07%	2.647	2.612	1.34%

Table 10. Separation Bubble Size Results (RDA).

Model	Baseline Size CFD	Min Size Resp. Surf.	Max Size Resp. Surf.
SA	0.467	0.441	0.507
W2006	0.535	0.522	0.672
SST	0.507	0.000	0.903

Table 11. Sobol Indices of Closure Coefficients for C_D (RDA).

SA Coefficient	Sobol Index	W2006 Coefficient	Sobol Index	SST Coefficient	Sobol Index
κ	8.51×10^{-1}	σ_w	7.26×10^{-1}	β^*	7.95×10^{-1}
σ	6.08×10^{-2}	β^*	2.07×10^{-1}	σ_{w1}	9.19×10^{-2}
c_{v1}	5.35×10^{-2}	C_{lim}	1.89×10^{-1}	β^*/β_1	7.96×10^{-2}
c_{w2}	2.56×10^{-2}			β^*/β_2	4.86×10^{-2}
c_{b1}	1.08×10^{-2}			a_1	3.01×10^{-3}
c_{w3}	3.17×10^{-5}				

$c = 1$). The separation bubble size results for the UQ analyses are included in Table 10. Originally, the SST response surface for separation bubble size yielded a negative minimum bubble size. This was due to the fact that for certain samples there was a very small, or even no separation region, yielding negative values for the response. Since this is not physical, the minimum value is set to zero.

The Sobol indices for C_D and separation bubble size agree well with the Sobol indices in the original analyses. These values are included in Tables 11 and 12. The ranking of importance is mostly the same between the original and reduced-dimensionality analyses. Even when the ranking of importance is not the same, the actual numeric values of the Sobol indices in the reduced-dimensionality analyses are still reasonably close to their corresponding values in the original analyses.

Response surfaces for pressure coefficient (C_p) and skin friction coefficient (C_f) were generated at each axial location across the bump. Sobol indices for these coefficients were also calculated at each axial location. The minimum and maximum possible values of C_p and C_f were calculated at each axial location from the response surfaces.

Plots of C_p versus x were generated for all of the cases used in the UQ analysis, for each turbulence model. This was done to verify the physical feasibility of the solutions. Each plot contains data for the baseline case; UQ training cases (green lines); minimum and maximum C_p bounds; and experimental data from Bachalo and Johnson.[4] The authors would like to emphasize that Bachalo and Johnson did not report any experimental uncertainty in their results, so the experimental data in these figures should be considered as reference only. A proper comparison with experiment should take into account the uncertainty both in the numerical model and experimental data, and the difference should be quantified with appropriate metrics for the validation of the numerical model.

The C_p versus x plots are included in Figs. 6a, 6c, and 6e. The Sobol indices for C_p versus x are included in Figs. 6b, 6d, and 6f. For clarity, only the Sobol indices of coefficients with significant contributions to uncertainty in C_p are shown in the figures. For each model, additional cases were run at the corners of

American Institute of Aeronautics and Astronautics

Table 12. Sobol Indices of Closure Coefficients for Separation Bubble Size (RDA).

SA		W2006		SST	
Coefficient	Sobol Index	Coefficient	Sobol Index	Coefficient	Sobol Index
σ	$5.79{\times}10^{-1}$	C_{lim}	$7.49{\times}10^{-1}$	β^*	$6.27{\times}10^{-1}$
κ	$1.84{\times}10^{-1}$	β^*	$2.71{\times}10^{-1}$	β^*/β_1	$1.86{\times}10^{-1}$
c_{w2}	$1.45{\times}10^{-1}$	σ_w	$7.63{\times}10^{-2}$	σ_{w1}	$1.37{\times}10^{-1}$
c_{b1}	$5.91{\times}10^{-2}$			β^*/β_2	$1.24{\times}10^{-1}$
c_{w3}	$3.27{\times}10^{-2}$			a_1	$7.99{\times}10^{-2}$
c_{v1}	$3.65{\times}10^{-3}$				

the hypercube defined by the epistemic interval bounds of only the most significant closure coefficients; this was done to eliminate the effect of discontinuities in the response surfaces near the shock and to determine the epistemic uncertainty interval for the output in the shock region only. The C_p minimum and maximum curves in Figs. 6a, 6c, and 6e are piece-wise combinations of the NIPC response surfaces and these hypercube cases in the shock region.

Note that each of the minimum and maximum C_p curves may not in general correspond to one flow solution each, because each point along each curve is calculated from either the response surface generated by using the C_p values of each UQ case at that specific x-location, or by one of the hypercube corner cases. While there exist flow solutions that pass through or very near to the minimum and maximum C_p curves at each point, there is no flow solution that passes through all of the minimum or all of the maximum points.

Plots of skin friction coefficient at each axial location were created in a similar fashion as the plots of pressure coefficient. Plots of C_f versus x for each UQ case are included in Figs. 7a, 7c, and 7e. As before, the minimum and maximum C_f curves in these figures are piece-wise combinations of the NIPC response surfaces at each axial location and hypercube corner samples in the shock region. The vertical lines in the plots are the separation and reattachment point locations reported by Bachalo and Johnson.[4] The Sobol indices for C_f at each axial location are shown in Figs. 7b, 7d, and 7f.

Based on the reduced-dimensionality results, all of the coefficients found to be significant to the axisymmetric transonic bump in Section V.A are indeed significant to their respective turbulence models, even in the absence of possible numerical "noise" caused by the insignificant coefficients in the original analyses. Of the three turbulence models, the SST model is most sensitive to changes in its closure coefficients; this is evidenced by large variations in the model's values for C_D and separation bubble size, as well as the large solution bands for C_p and C_f. The SA and W2006 models are roughly equally sensitive to changes in their closure coefficients. All of the models are most sensitive to changes in their closure coefficients in the shock and separated regions of the flow, particularly so in the latter region. None of the models exhibit large uncertainties in C_p upstream of the shock or downstream of the reattachment point, however the uncertainty in C_f remains large in these regions.

V.C. RAE 2822 Airfoil - Original Analyses

As with the original analyses of the transonic bump, the purpose of the original analyses of the RAE 2822 airfoil was to identify the closure coefficients that contribute significantly to uncertainty in the output quantities of interest. For the RAE 2822, the output quantities of interest include the lift coefficient (C_L), drag coefficient due to pressure ($C_{D_{\mathrm{press}}}$), drag coefficient due to skin friction ($C_{D_{\mathrm{sf}}}$), and pressure coefficient distribution (C_p). The skin friction coefficient distribution was not investigated for the RAE 2822 because no separation bubble was observed in the baseline case solutions.

In the same manner as for the transonic bump, Sobol indices were calculated for the output quantities of interest of the RAE 2822. The results for C_L, $C_{D_{\mathrm{press}}}$, and $C_{D_{\mathrm{sf}}}$ are included in Tables 13, 14, and 15 respectively.

For the SA model, the largest contributors to uncertainty in C_L are κ, c_{t4}, c_{t3}, c_{v1}, and c_{b1}. The largest contributors to uncertainty in $C_{D_{\mathrm{press}}}$ are σ, c_{w2}, c_{b1}, and c_{t4}; and the largest contributors to uncertainty in $C_{D_{\mathrm{sf}}}$ are κ, σ, c_{w2}, c_{t4}, c_{t3}, and c_{v1}.
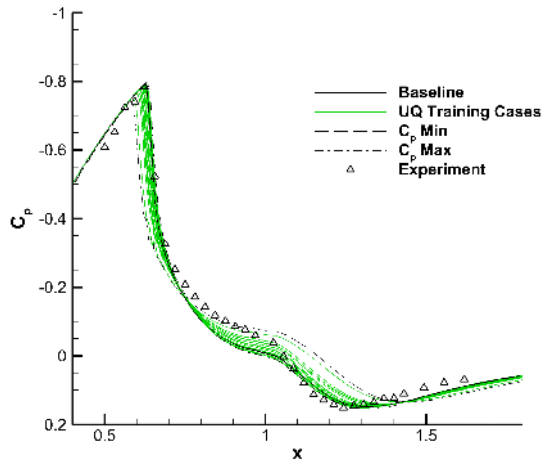
For the W2006 model, the largest contributors to uncertainty in all three integrated quantities are C_{lim},
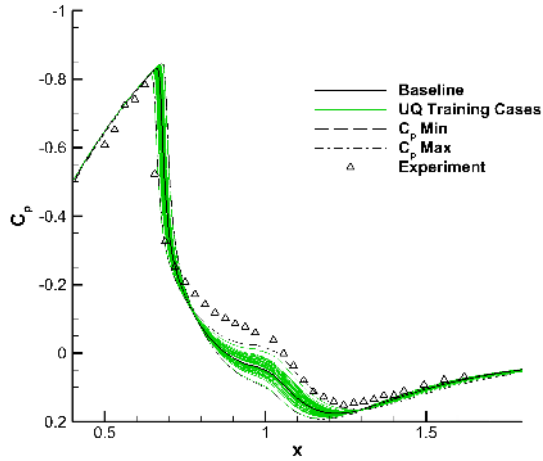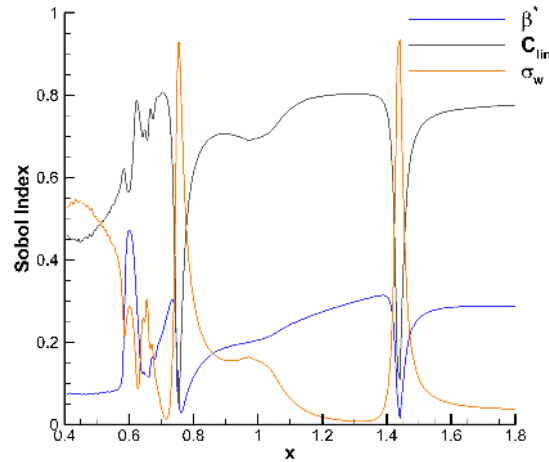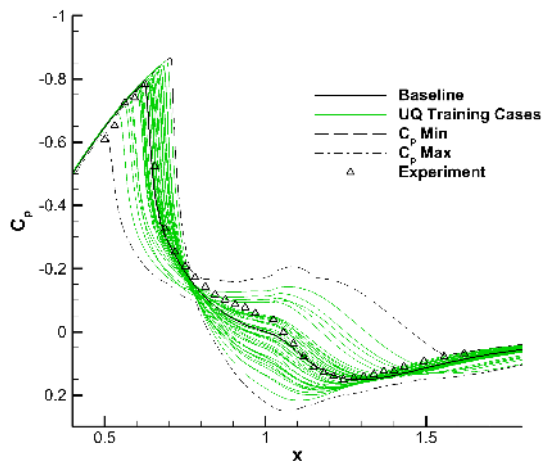
(a) C_p versus x (SA).
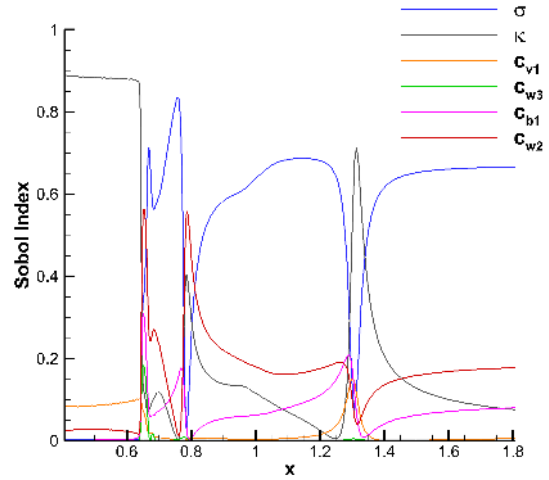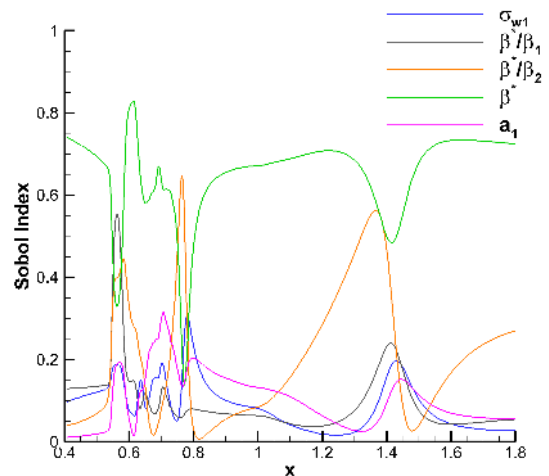
(b) Sobol indices for C_p versus x (SA).

(c) C_p versus x (W2006).

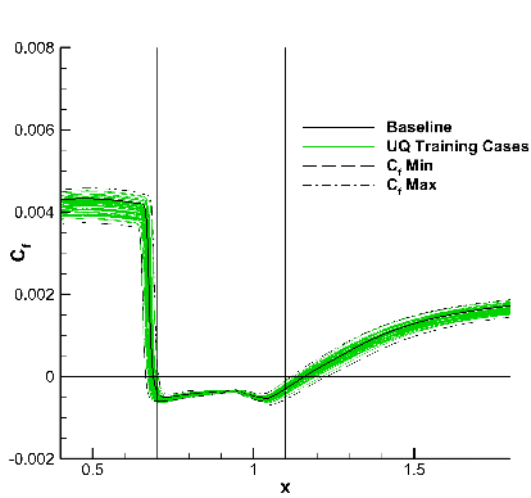(d) Sobol indices for C_p versus x (W2006).
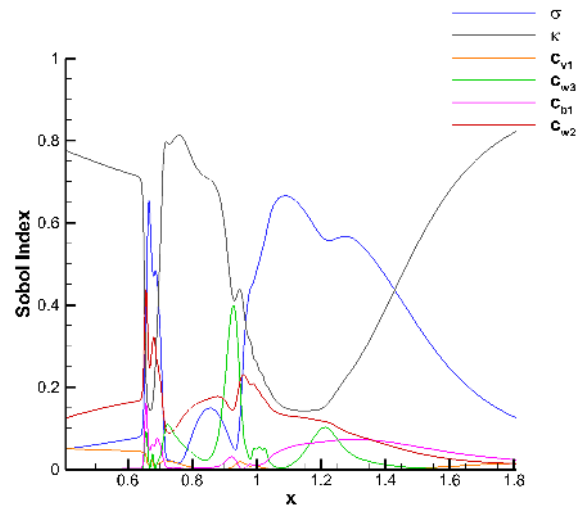
(e) C_p versus x (SST).

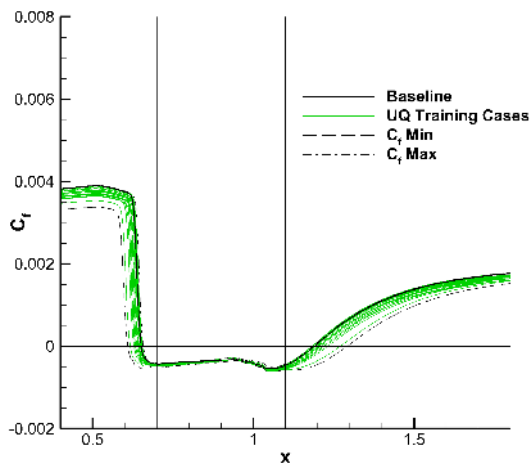(f) Sobol indices for C_p versus x (SST).

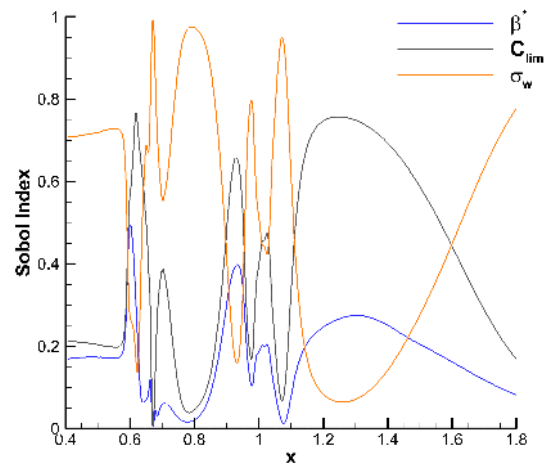Figure 6. Pressure coefficient results for transonic bump.
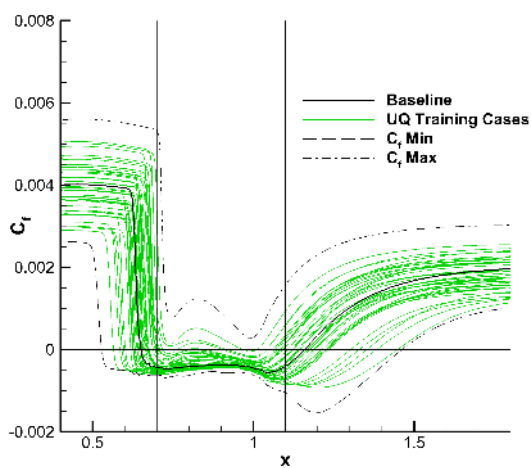
(a) C_f versus x (SA).

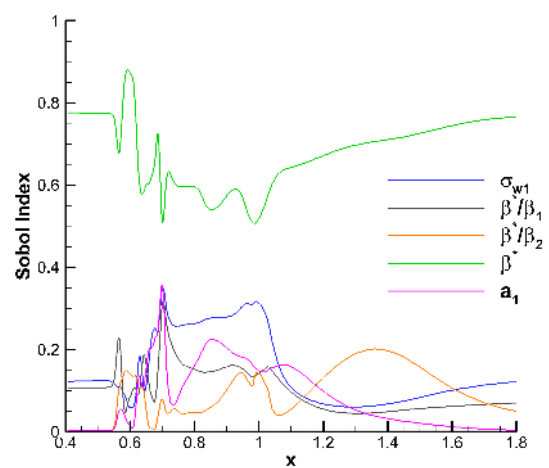(b) Sobol indices for C_f versus x (SA).

(c) C_f versus x (W2006).

(d) Sobol indices for C_f versus x (W2006).

(e) C_f versus x (SST).

(f) Sobol indices for C_f versus x (SST).

Figure 7. Skin friction coefficient results for transonic bump.

American Institute of Aeronautics and Astronautics

Table 13. Sobol Indices of Closure Coefficients for C_L of RAE 2822.

SA		W2006		SST	
Coefficient	Sobol Index	Coefficient	Sobol Index	Coefficient	Sobol Index
κ	5.07×10^{-1}	C_{lim}	8.55×10^{-1}	β^*/β_2	4.22×10^{-1}
c_{t4}	2.34×10^{-1}	β^*	9.57×10^{-2}	a_1	4.13×10^{-1}
c_{t3}	1.82×10^{-1}	σ_w	4.23×10^{-2}	β^*	2.50×10^{-1}
c_{v1}	7.30×10^{-2}	κ	1.83×10^{-2}	σ_{w2}	2.37×10^{-2}
c_{b1}	3.18×10^{-2}	β^*/β_0	1.27×10^{-2}	σ_{w1}	1.64×10^{-2}
c_{w2}	1.78×10^{-2}	σ_k	1.19×10^{-2}	β^*/β_1	1.59×10^{-2}
σ	1.55×10^{-2}			σ_{k2}	1.11×10^{-2}
c_{b2}	1.51×10^{-2}			σ_{k1}	9.95×10^{-3}
c_{w3}	9.52×10^{-3}			κ	8.63×10^{-3}
c_{t1}	8.12×10^{-3}				
c_{t2}	6.13×10^{-3}				

Table 14. Sobol Indices of Closure Coefficients for C_{D_press}.

SA		W2006		SST	
Coefficient	Sobol Index	Coefficient	Sobol Index	Coefficient	Sobol Index
σ	4.64×10^{-1}	C_{lim}	6.62×10^{-1}	β^*	6.30×10^{-1}
c_{w2}	2.13×10^{-1}	σ_w	2.14×10^{-1}	β^*/β_2	2.36×10^{-1}
c_{b1}	1.91×10^{-1}	β^*	1.71×10^{-1}	a_1	1.34×10^{-1}
c_{t4}	7.10×10^{-2}	β^*/β_0	4.81×10^{-3}	β^*/β_1	3.22×10^{-2}
c_{v1}	2.90×10^{-2}	κ	2.46×10^{-3}	σ_{w1}	1.18×10^{-2}
κ	2.74×10^{-2}	σ_k	2.32×10^{-3}	σ_{w2}	1.11×10^{-2}
c_{t3}	2.07×10^{-2}			σ_{k2}	4.99×10^{-3}
c_{b2}	1.25×10^{-2}			σ_{k1}	4.71×10^{-3}
c_{t2}	7.16×10^{-3}			κ	1.95×10^{-3}
c_{t1}	5.01×10^{-3}				
c_{w3}	3.90×10^{-3}				

β^*, and σ_w. The order of importance is different for C_L, C_{D_press}, and C_{D_sf}, but the important coefficients are the same for each quantity.

For the SST model, the largest contributors to uncertainty in C_L are β^*/β_2, a_1, and β^*. The largest contributors to uncertainty in C_{D_press} are β^*, β^*/β_2, a_1, and $\beta^*\beta_1$; and the largest contributors to uncertainty in C_{D_sf} are β^*, σ_{w1}, and β^*/β_1.

Response surfaces for C_p were generated at each x-location on the top and bottom surface of the airfoil so that the closure coefficients with significant contributions to C_p at any given point in the flow could be identified. These plots are included in Fig. 8. In Fig. 8a, the largest contributor to uncertainty in C_p for the majority of the x domain in the SA model is κ. There are also spikes in the Sobol indices of c_{t3}, c_{t4}, and σ, indicating that these coefficients are also important in some parts of the flow; particularly, spikes appear near the shock on the upper surface and near the high-pressure region at the leading edge on the lower surface. In Fig. 8b, the uncertainty in C_p for the W2006 model is almost completely dominated by C_{lim}, with only a few minor contributions from β^* and σ_2. In Fig. 8c, the uncertainty in C_p for the SST model is mostly attributed to β^*/β_2, β^*, and a_1. At $x \approx 0.6$, σ_{w1} also has a minor contribution.

In sum, seven closure coefficients were found to contribute significantly to at least one output quantity of interest for the SA model; three coefficients for the W2006 model; and five coefficients for the SST model. This information is summarized in Table 16.

American Institute of Aeronautics and Astronautics
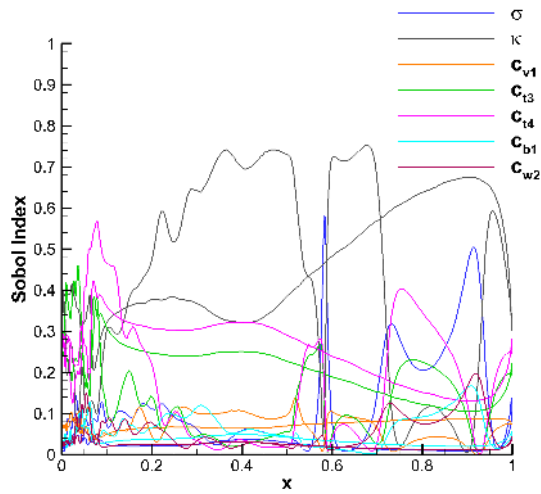
(a) Sobol indices for C_p versus x (SA).
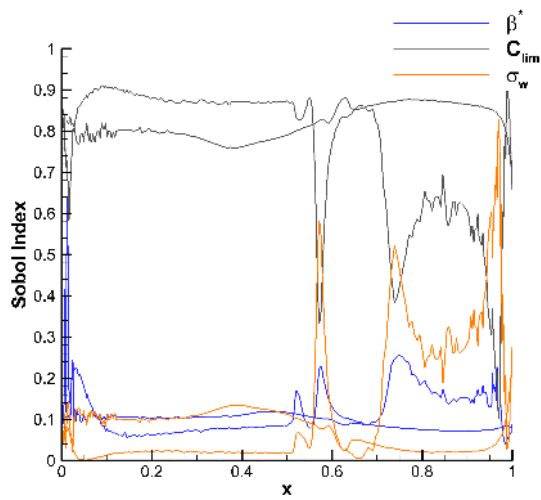
(b) Sobol indices for C_p versus x (W2006).
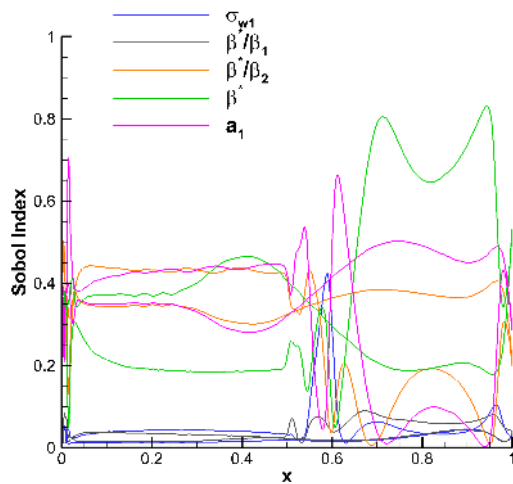
(c) Sobol indices for C_p versus x (SST).

Figure 8. Sobol index distributions for RAE 2822 airfoil (Original Analyses).

American Institute of Aeronautics and Astronautics

Table 15. Sobol Indices of Closure Coefficients for $C_{D_{\mathrm{sf}}}$.

	SA		W2006		SST
Coefficient	Sobol Index	Coefficient	Sobol Index	Coefficient	Sobol Index
κ	5.65×10^{-1}	σ_w	6.41×10^{-1}	β^*	7.75×10^{-1}
σ	2.36×10^{-1}	C_{lim}	2.39×10^{-1}	σ_{w1}	1.22×10^{-1}
c_{w2}	8.50×10^{-2}	β^*	1.56×10^{-1}	β^*/β_1	9.50×10^{-2}
c_{t4}	4.30×10^{-2}	κ	1.07×10^{-2}	a_1	9.84×10^{-3}
c_{t3}	3.58×10^{-2}	σ_k	9.71×10^{-3}	β^*/β_2	5.32×10^{-3}
c_{v1}	3.06×10^{-2}	β^*/β_0	3.59×10^{-3}	σ_{w2}	1.17×10^{-3}
c_{b1}	1.97×10^{-2}			σ_{k1}	8.58×10^{-4}
c_{b2}	1.65×10^{-3}			σ_{k2}	8.34×10^{-4}
c_{t1}	1.36×10^{-3}			κ	1.30×10^{-4}
c_{w3}	1.17×10^{-3}				
c_{t2}	6.17×10^{-4}				

Table 16. Closure Coefficients with Significant Contributions to RAE 2822.

SA	W2006	SST
σ	β^*	σ_{w1}
κ	C_{lim}	β^*/β_1
c_{v1}	σ_w	β^*/β_2
c_{t3}		β^*
c_{t4}		a_1
c_{b1}		
c_{w2}		

V.D.   RAE 2822 Airfoil - Reduced Dimensionality Analyses

As with the transonic bump, a reduced-dimensionality analysis was performed on the RAE 2822 for each of the turbulence models to further improve the accuracy of the response surfaces used in the uncertainty analyses. A baseline case was run with each of the original, unchanged turbulence models for the RAE 2822 airfoil. The response surfaces of drag coefficient and lift coefficient for the RAE 2822 were verified in the same manner as the response surfaces of the drag coefficient of the transonic bump; the minimum and maximum values of C_D and C_L were first calculated from the response surfaces, and then CFD simulations were run by using the closure coefficients that produced these minimum and maximum values. The comparison between the response surfaces and CFD is summarized in Tables 17 and 18. All of the C_D response surfaces are within 4.37% or less of the CFD, and the C_L response surfaces are within 1.18% or less of the CFD.

The Sobol indices for C_L, $C_{D_{\mathrm{press}}}$, and $C_{D_{\mathrm{sf}}}$ agree well with the Sobol indices in the original analyses. The results for the reduced-dimensionality analyses are included in Tables 19, 20, and 21. As with the transonic bump, the ranking of importance of the closure coefficients for each quantity is mostly the same between

Table 17. RAE 2822 Drag Coefficient Results, in Drag Counts (RDA).

	Baseline C_D	Min C_D			Max C_D		
Model	CFD	Resp. Surf.	CFD	Difference	Resp. Surf.	CFD	Difference
SA	146.0	134.7	135.8	0.81%	152.8	151.2	1.06%
W2006	142.3	130.2	128.5	1.32%	144.4	144.4	0.00%
SST	128.5	107.2	112.1	4.37%	183.0	182.8	0.11%

American Institute of Aeronautics and Astronautics

Table 18. RAE 2822 Lift Coefficient Results (RDA).

Model	Baseline C_L CFD	Min C_L Resp. Surf.	Min C_L CFD	Min C_L Difference	Max C_L Resp. Surf.	Max C_L CFD	Max C_L Difference
SA	0.744	0.735	0.739	0.57%	0.769	0.764	0.69%
W2006	0.744	0.733	0.738	0.68%	0.749	0.748	0.13%
SST	0.744	0.710	0.719	1.18%	0.778	0.774	0.45%

Table 19. Sobol Indices of Closure Coefficients for C_L of RAE 2822 (RDA).

SA Coefficient	SA Sobol Index	W2006 Coefficient	W2006 Sobol Index	SST Coefficient	SST Sobol Index
κ	5.09×10^{-1}	C_{lim}	8.96×10^{-1}	a_1	5.21×10^{-1}
c_{t4}	2.18×10^{-1}	β^*	9.93×10^{-2}	β^*/β_2	3.27×10^{-1}
c_{t3}	1.81×10^{-1}	σ_w	1.84×10^{-2}	β^*	2.81×10^{-1}
c_{v1}	1.03×10^{-1}			β^*/β_1	1.10×10^{-1}
σ	2.83×10^{-2}			σ_{w1}	4.48×10^{-2}
c_{b1}	2.60×10^{-2}				
c_{w2}	2.23×10^{-2}				

the original and reduced-dimensionality analyses. Even when the ranking of importance is not the same, the actual numeric values of the Sobol indices in the reduced-dimensionality analyses are still reasonably close to their corresponding values in the original analyses.

Pressure coefficient plots were generated for each turbulence model. Each of the plots contains data for the baseline case; UQ training cases (green lines); the minimum and maximum C_p bounds; and experimental data from Cook et al.[9] Cook et al. did not report any experimental uncertainty, so the experimental results are included as reference only. The C_p versus x plots are included in Figs. 9a, 9c, and 9e; and the Sobol indices for C_p versus x are included in Figs. 9b, 9d, and 9f. For clarity, only the Sobol indices of coefficients with significant contributions to uncertainty in C_p are shown in the figures. Similarly to the transonic bump, the minimum and maximum C_p curves Figs. 9a, 9c, and 9e are piece-wise combinations of the NIPC response surfaces and cases run at the corners of the hypercubes defined by the epistemic bounds of the closure coefficients in the shock region.

Based on the reduced-dimensionality results, all of the coefficients found to be significant to the RAE 2822 airfoil in Section V.C are indeed significant to their respective turbulence models. Of the three models, the SST model is most sensitive to changes in its closure coefficients, as evidenced by its larger variations in C_L, C_{D_press}, and C_{D_sf}, and by its larger solution band for C_p compared to the SA and W2006 models. The SA and W2006 models are roughly equally sensitive to changes in their closure coefficients, with the latter particularly insensitive. All of the models are most sensitive to changes in their closure coefficients in the shock region; everywhere else, there is very little uncertainty in C_p.

V.E. Comparison of Uncertainty Quantification Results Between the Two CFD Cases

The uncertainty quantification and sensitivity results of the axisymmetric transonic bump and RAE 2822 airfoil are consistent with one another. For the W2006 and SST models, every closure coefficient which is significant to at least one output quantity of interest for the transonic bump is also significant to at least one output quantity of interest for the RAE 2822 and vice versa. This agreement is nearly observed by the SA model as well, with only one coefficient significant to the transonic bump but not the RAE 2822, and only two coefficients significant to the RAE 2822, but not the transonic bump. A summary of all of the significant closure coefficients is included in Fig. 10.
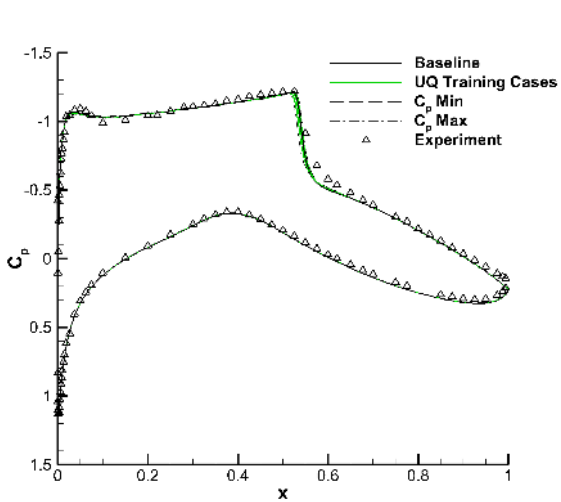
Compared to the transonic bump results, the RAE 2822 results are much less sensitive to changes in all three turbulence models' closure coefficients. The same trends still apply however; the SST model is most sensitive to changes in its closure coefficients, and the SA and W2006 models are roughly equally sensitive
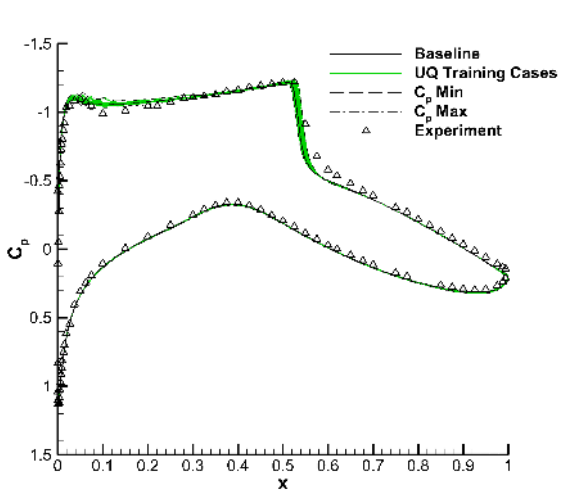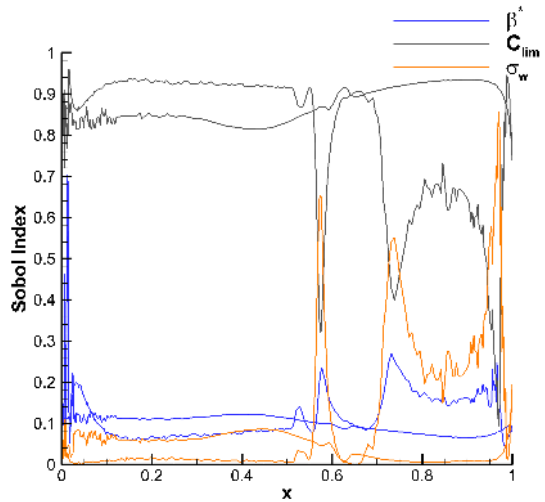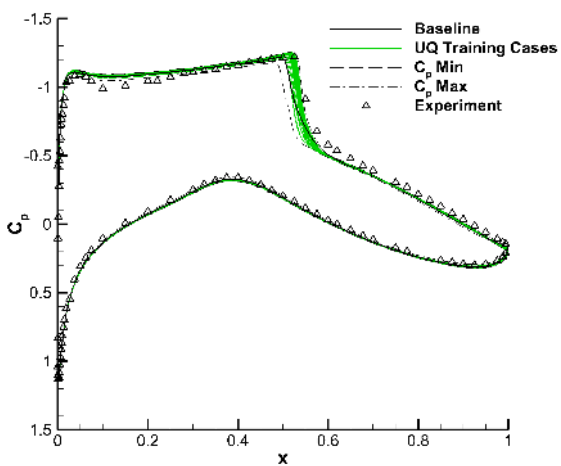
(a) C_p versus x (SA).
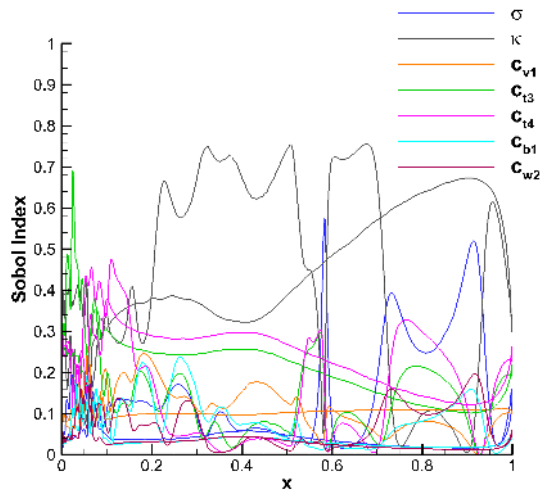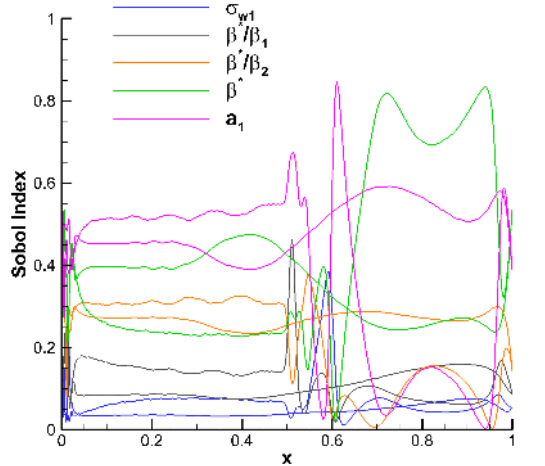
(b) Sobol indices for C_p versus x (SA).

(c) C_p versus x (W2006).

(d) Sobol indices for C_p versus x (W2006).

(e) C_p versus x (SST).

(f) Sobol indices for C_p versus x (SST).

Figure 9. Pressure coefficient results for RAE 2822.

American Institute of Aeronautics and Astronautics

Table 20. Sobol Indices of Closure Coefficients for $C_{D_{\text{press}}}$ of RAE 2822 (RDA).

SA		W2006		SST	
Coefficient	Sobol Index	Coefficient	Sobol Index	Coefficient	Sobol Index
σ	4.55×10^{-1}	C_{lim}	7.01×10^{-1}	β^*	6.64×10^{-1}
c_{b1}	2.24×10^{-1}	β^*	1.82×10^{-1}	β^*/β_2	2.02×10^{-1}
c_{w2}	2.23×10^{-1}	σ_w	1.64×10^{-1}	a_1	1.77×10^{-1}
c_{t4}	5.26×10^{-2}			β^*/β_1	5.15×10^{-2}
κ	4.27×10^{-2}			σ_{w1}	2.19×10^{-2}
c_{v1}	3.19×10^{-2}				
c_{t3}	2.17×10^{-2}				

Table 21. Sobol Indices of Closure Coefficients for $C_{D_{\text{sf}}}$ of RAE 2822 (RDA).

SA		W2006		SST	
Coefficient	Sobol Index	Coefficient	Sobol Index	Coefficient	Sobol Index
κ	5.69×10^{-1}	σ_w	6.92×10^{-1}	β^*	7.91×10^{-1}
σ	2.33×10^{-1}	C_{lim}	2.10×10^{-1}	σ_{w1}	1.15×10^{-1}
c_{w2}	8.30×10^{-2}	β^*	1.45×10^{-1}	β^*/β_1	9.10×10^{-2}
c_{t4}	4.25×10^{-2}			a_1	1.09×10^{-2}
c_{v1}	4.05×10^{-2}			β^*/β_2	3.68×10^{-3}
c_{t3}	3.52×10^{-2}				
c_{b1}	1.89×10^{-2}				

to changes in their closure coefficients. Uncertainties in C_p are particularly large in the shock region of each flow for all three turbulence models.

The information presented in this paper is expected to be of interest to the CFD community because it demonstrates that large changes in turbulence model behavior can be observed by changing specific sets of closure coefficients. In particular, there are two main results that can enable the advancement of turbulence models used in RANS simulations. The first result is that if improved matching between CFD and experiments (i.e., the data representing the real physical phenomena) is desired, the Sobol indices presented in this work for certain output quantities of interest give clues for which closure coefficients to modify first. The second result is that if the aerospace community can reduce the uncertainty in only a certain set of closure coefficients (whether through experimentation, LES/DES, etc.), the uncertainty in turbulence model predictions can be greatly reduced. For example, the uncertainty in the value of Von Kármán's constant in the SA model was responsible for approximately 85% of the uncertainty in C_D of the axisymmetric transonic bump. If more information were known about the true value of κ, the results of the SA model would be much less uncertain.

If improved accuracy is desired, a good starting point may be to first consider the integrated quantities; that is, C_D for the axisymmtaric transonic bump, and C_L, $C_{D_{\text{press}}}$, and $C_{D_{\text{sf}}}$ for the RAE 2822 airfoil. Referring back to Tables 11, 19, 20, and 21, a small number of closure coefficients can be identified for each turbulence model which consistently contribute to very large amounts to uncertainty in the output quantities of interest. These coefficients include κ and σ for the SA model; C_{lim} and σ_w for the W2006 model; and β^* for the SST model. The authors suggest that these coefficients be considered first in future refinements of the turbulence models discussed here.

VI. Conclusions and Future Work

Two detailed uncertainty quantification studies focusing on turbulence model closure coefficients were performed on an axisymmetric transonic bump at zero degrees angle of attack and the RAE 2822 transonic airfoil at a lift coefficient of 0.744. The transonic bump has freestream $M = 0.875$ and $Re = 2.763 \times 10^6$,

(a) SA - Significant closure coefficients.

(b) W2006 - Significant closure coefficients.

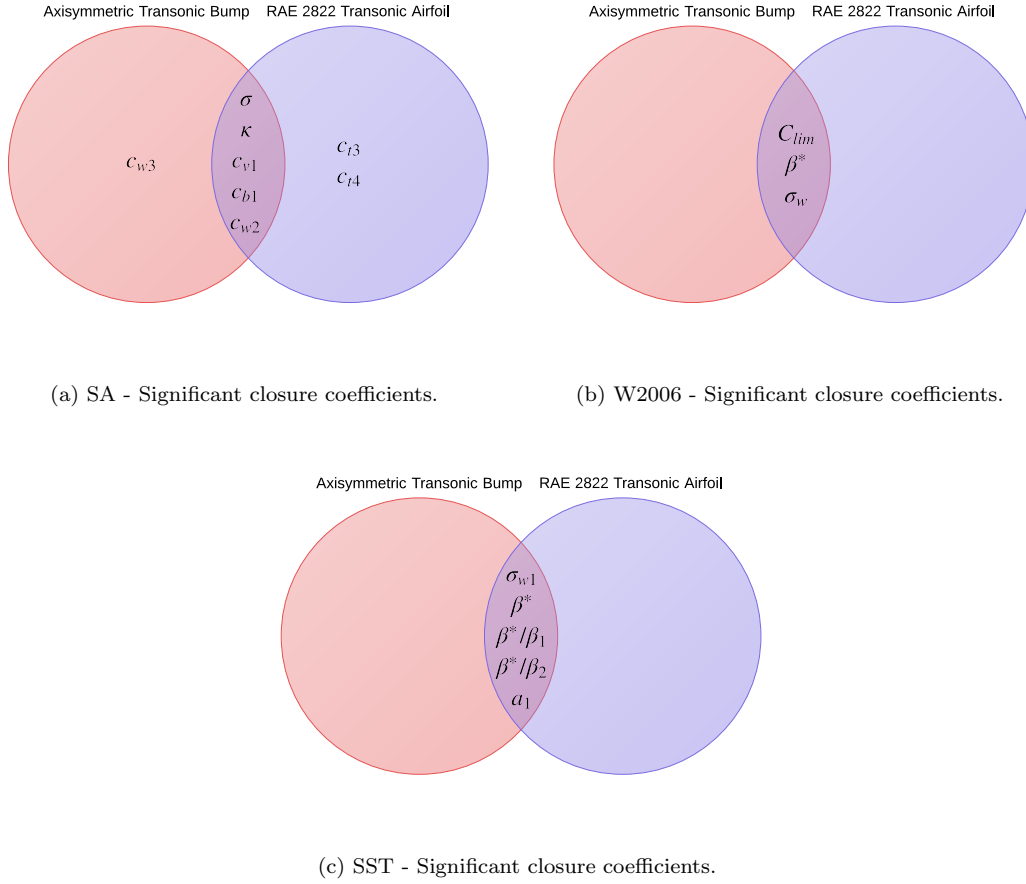(c) SST - Significant closure coefficients.

Figure 10.   Closure coefficients significant to uncertainty in at least one output quantity of interest for each CFD problem and for each turbulence model.

and the RAE 2822 has freestream $M = 0.729$ and $Re = 6.5 \times 10^6$. The turbulence models considered were the Spalart-Allmaras Model, Wilcox (2006) k-ω Model, and Menter Shear-Stress Transport Model. The uncertainty quantification employed stochastic expansions based on non-intrusive polynomial chaos as an efficient means of uncertainty propagation. The drag coefficient, wall pressure and skin friction coefficient distributions, and shock-induced separation bubble size were considered as uncertain outputs for the transonic bump. The lift coefficient, pressure and skin friction components of drag coefficient, and wall pressure coefficient distribution were considered as uncertain outputs for the RAE 2822. Sobol indices were used to rank the relative contributions of each closure coefficient to the total uncertainty in the output quantities of interest. This information can be used a potential starting point in the future advancement of the turbulence models considered here, and it is a first step towards quantifying model-form uncertainty.

Based on the results, the following conclusions can be made: For the SA model, the coefficients that contribute most to uncertainty in the output quantities of interest are σ, κ, c_{v1}, c_{b1}, c_{w2}, c_{t3}, c_{t4}, and c_{w3}. For the W2006 model, the coefficients that contribute most to uncertainty in the output quantities of interest are β^*, C_{lim}, and σ_w. For the SST model, the coefficients that contribute most to uncertainty in the output quantities of interest are σ_{w1}, β^*/β_1, β^*/β_2, β^*, and a_1. With the exception of c_{w3}, c_{t3}, and c_{t4} in the SA model, all other closure coefficients were found to be significant to both the axisymmetric transonic bump and RAE 2822 transonic airfoil.

In the future refinement of the models discussed here, the authors suggest that studies should focus on increasing knowledge of appropriate values for κ and σ for the SA model; C_{lim} and σ_w for the W2006 model; and β^* for the SST model. Improved knowledge of the values of these particular closure coefficients

American Institute of Aeronautics and Astronautics

will have the largest impact on reducing the uncertainty in integrated quantities of interest for the RANS simulations of wall-bounded transonic flows. Future work should also focus on determining why certain closure coefficients contribute more or less to uncertainty at different flow locations. For example, research should be done to determine why σ in the SA model becomes important to C_f for the transonic bump after the reattachment point, but not before. Finally, future work should include more CFD problems, particularly in three dimensions.

Acknowledgments

References

[1]Spalart, P. R. and Allmaras, S. R., "A One-Equation Turbulence Model for Aerodynamic Flows," *Recherche Aerospatiale*, No. 1, 1994, pp. 5-21.

[2]Wilcox, D. C., "Formulation of the k-omega Turbulence Model Revisited," *AIAA Journal*, Vol. 46, No. 11, 2008, pp. 2823-2828.

[3]Menter, F. R., "Two-Equation Eddy-Viscosity Turbulence Models for Engineering Applications," *AIAA Journal*, Vol. 32, No. 8, August 1994, pp. 1598-1605.

[4]Bachalo, W. D. and Johnson, D. A., "Transonic, Turbulent Boundary-Layer Separation Generated on an Axisymmetric Flow Model," *AIAA Journal*, Vol. 24, No. 3, 1986, pp. 437-443.

[5]Hosder, S., Walters, R. W., and Balch, M., "Point-Collocation Nonintrusive Polynomial Chaos Method for Stochastic Computational Fluid Dynamics," *AIAA Journal*, Vol. 48, No. 12, December 2010.

[6]Sudret, B., "Global sensitivity analysis using polynomial chaos expansion," *Reliability Engineering and System Safety*, Vol. 93, No. 7, 2008, pp. 964-979.

[7]Biedron, R. T., Derlaga, J. M., Gnoffo, P. A., Hammond, D. P., Jones, W. T., Kleb, B., Lee-Rausch, E. M., Nielsen, E. J., Park, M. A., Rumsey, C. L., Thomas, J. L., and Wood, W. A., "FUN3D Manual: 12.4," NASA/TM-2014-218179, March 2014.

[8]"NASA Langley Research Center Turbulence Modeling Resource," http://turbmodels.larc.nasa.gov [retrieved April 2015].

[9]Cook, P.H., McDonald, M.A., and Firmin, M.C.P., "Aerofoil RAE 2822 - Pressure Distributions, and Boundary Layer and Wake Measurements," *Experimental Data Base for Computer Program Assessment*, AGARD Report AR 138, 1979.

[10]Nee, V. W. and Kovasznay, L. S. G., "The Calculation of the Incompressible Turbulent Boundary Layer by a Simple Theory," *Physics of Fluids*, Vol. 12, 1968, pp. 473.

[11]Bailey, S. C. C., Vallikivi, M., Hultmark, M., and Smits, A. J., "Estimating the value of von Kármán's constant in turbulent pipe flow," *Journal of Fluid Mechanics*, Vol. 749, 2014, pp. 79-98.

[12]Email correspondence between Philippe Spalart and John Schaefer, June-December 2014.

[13]Wilcox, D. C., *Turbulence Modeling for CFD*, 3rd edition, DCW Industries, Inc., La Cañada CA, 2006.

[14]Email correspondence between David Wilcox and John Schaefer, June 2014.

[15]Georgiadis, N. J. and Yoder, D. A., "Recalibration of the Shear Stress Transport Model to Improve Calculation of Shock Separated Flows," AIAA Paper 2013-0685, January 2013.

[16]Email correspondence between Florian Menter and John Schaefer, June 2014.

[17]West, T. K. and Hosder, S., "Uncertainty Quantification of Hypersonic Reentry Flows with Sparse Sampling and Stochastic Expansions," *Journal of Spacecraft and Rockets*, Vol. 52, No. 1, January-February 2015, pp. 120-133.

[18]Ghanem, R. G. and Spanos, P. D., "Stochastic Finite Elements: A Spectral Approach," Springer-Verlag, New York, 1991.

[19]Eldred, M. S., "Recent Advances in Non-Intrusive Polynomial Chaos and Stochastic Collocation Methods for Uncertainty Analysis and Design," AIAA Paper 2009-2274, May 2009.

[20]Hosder, S., Walters, R. W., and Balch, M., "Efficient Sampling for Non-Intrusive Polynomial Chaos Applications with Multiple Input Uncertain Variables," AIAA-Paper 2007-1939, April 2007.

[21]Crestaux, T., Maitre, O. L., and Martinez, J.-M, "Polynomial chaos expansion for sensitivity analysis," *Reliability Engineering and System Safety*, 2009.

[22]Ghaffari, S., Magin, T., and Iaccarino, G., "Uncertainty Quantification of Radiative Heat Flux Modeling for Titan Atmospheric Entry," AIAA Paper 2010-239, January 2010.

American Institute of Aeronautics and Astronautics

Appendix A: Sobol Index Derivation

In this section, the derivation of Sobol indices is presented. First, the total variance, D, can be written in terms of the PCE as shown in Eq. (37).

$$D = \sum_{j=1}^{P} \alpha_j^2(t, \vec{x}) \left\langle \Psi_j^2(\vec{\xi}) \right\rangle \tag{37}$$

Then, as shown by Sudret[6] and Crestaux et al.,[21] the total variance can be decomposed as:

$$D = \sum_{i=1}^{i=n} D_i + \sum_{1 \leq i < j \leq n}^{i=n-1} D_{i,j} + \sum_{1 \leq i < j < k \leq n}^{i=n-2} D_{i,j,k} + \cdots + D_{1,2,\ldots,n} \tag{38}$$

where the partial variances $(D_{i_1,\ldots,i_s})$ are given by:

$$D_{i_1,\ldots,i_s} = \sum_{\beta \in \{i_1,\ldots,i_s\}} \alpha_\beta^2 \left\langle \Psi_\beta^2(\vec{\xi}) \right\rangle, \qquad 1 \leq i_1 < \ldots < i_s \leq n \tag{39}$$

Then the Sobol indices $(S_{i_1 \cdots i_s})$ are defined as,

$$S_{i_1 \cdots i_s} = \frac{D_{i_1,\ldots,i_s}}{D} \tag{40}$$

which satisfy the following equation:

$$\sum_{i=1}^{i=n} S_i + \sum_{1 \leq i < j \leq n}^{i=n-1} S_{i,j} + \sum_{1 \leq i < j < k \leq n}^{i=n-2} S_{i,j,k} + \cdots + S_{1,2,\ldots,n} = 1.0 \tag{41}$$

The Sobol indices provide a sensitivity measure due to individual contribution from each input uncertain variable (S_i), as well as the mixed contributions $(\{S_{i,j}\}, \{S_{i,j,k}\}, \cdots)$. As shown by Sudret[6] and Ghaffari et al.,[22] the total (combined) effect (S_{T_i}) of an input parameter i is defined as the summation of the partial Sobol indices that include the particular parameter:

$$S_{T_i} = \sum_{L_i} \frac{D_{i_1,\ldots,i_s}}{D}; \quad L_i = \{(i_1,\ldots,i_s) : \exists\, k,\ 1 \leq k \leq s,\ i_k = i\} \tag{42}$$

For example, with $n = 3$, the total contribution to the overall variance from the first uncertain variable $(i = 1)$ can be written as:

$$S_{T_1} = S_1 + S_{1,2} + S_{1,3} + S_{1,2,3} \tag{43}$$

From these formulations, it can be seen that the Sobol indices can be used to provide a relative ranking of each input uncertainty to the overall variation in the output with the consideration of nonlinear correlation between input variables and output quantities of interest.

American Institute of Aeronautics and Astronautics